Failure Mechanism of Pb-Bearing and Pb-Free Solder Joints under High-Speed Shear Loading

Jong-Woong Kim[1] and Seung-Boo Jung[2,*]

[1]Display Research and Development Division, Korea Electronics Technology Institute
68 Yatap-dong, Bundang-gu, Seongnam-si, Gyeonggi 463-816, Korea
[2]School of Advanced Materials Science & Engineering, Sungkyunkwan University
300 Cheoncheon-dong, Jangan-gu, Suwon-si, Gyeonggi 440-746, Korea

The failure behaviors of ball grid array (BGA) solder ball joints under the various loading speeds of the high-speed shear test were investigated both experimentally and with non-linear, 3-dimensional finite element modeling. Conventional Sn-37Pb and Pb-free, Sn-3.5Ag solder alloys were used to compare the failure behaviors. Far greater shear forces were measured by the high-speed shear test than by the low-speed shear test. The shear force further increased with increasing shear speed, mainly due to the high strain-rate sensitivity of the solder alloys. Brittle interfacial fractures were more easily achieved by the high-speed shear test in the Sn-3.5Ag solder joints, especially at higher shear speed. This result was discussed in terms of the relationship between the strain-rate of the solder alloy, the work-hardening effect, and the resulting stress concentration in the interfacial regions. However, no transition of the failure mode was observed in the high-speed shear test of the Sn-37Pb solder joints.

Keywords: alloys, soldering, mechanical properties, computer simulation, high-speed shear test

1. INTRODUCTION

Currently, the most popular method to evaluate the mechanical joint reliability of the solder ball joint is the ball shear test due to its simple and convenient implementation. However, the ball shear test is not considered suitable for predicting the joint reliability under drop loading, as the applied test speeds, usually lower than 5 mm/s, are far below the impact velocities applied to the solder joint in a drop test. Recently, a modified solder ball shear tester that is capable of performing high-speed shearing of up to several meters per second was developed, suggesting that the complicated, board-level drop test might be replaced by the new, high-speed solder ball shear test [1-6]. With the possibility of high-speed shearing of the solder ball joint, the Joint Electronic Device Engineering Council (JEDEC) solder ball shear test standard, JESD22-B117, was also updated with the addition of 'A' at the end of the standard code to become JESD22-B117A, in October 2006 [7]. The incorporation of the high-speed shear test conditions was a significant addition to the standard. However, the shear speed, which is the displacement rate of a shear ram, has not yet been fully standardized with only a range being specified for the shear speed from 0.01 m/s to 1 m/s for the high-speed shear test. In our previous studies considering the effect of the shear speed in the low-speed shear test, we confirmed the significant effects exerted by this parameter on the shear force value and failure mode [8-10]. Therefore, the effect of this parameter on the high-speed shear test needs to be systemically investigated to elucidate the failure behaviors of the solder joints and their mechanisms under high-speed loading.

The JESD22-B117A also specifies the shear failure modes for the acceptance criteria of the solder ball joint. The primary impetus for including the failure mode is to screen the type of brittle interfacial fractures caused by excessively thick intermetallic compound (IMC) layers. During soldering, the solder alloy melts and then reacts with the metallization of the substrate to form IMCs at the joining interface. While forming a thin IMC layer, the achievement of a good metallurgical bond is desirable. However, an excessively thick reaction layer is very sensitive to stress and provides sites of initiation and paths for crack propagation because of the brittle layer and the microstructural mismatch between the solder and pad metallization. Dynamic loads under drop or impact conditions on the solder joint devices are another critical factor influencing the brittle failure mode. However, during the ball grid array (BGA) ball shear test, the sidewalls

*Corresponding author: sbjung@skku.ac.kr

of the solder mask tend to support the solder joint, which can alter the failure mode and, thus, introduce error into the shear test monitoring of the susceptibility to brittle interfacial failures.

The objective of this study was to evaluate the effect of an important high-speed shear test parameter, shear speed, on the shear force and failure behavior. A representative Pb-free solder, Sn-3.5Ag, was used to observe the effects in comparison to those of a conventional Sn-37Pb solder in terms of the failure behaviors of the BGA solder joints. Both an experimental investigation and a 3-dimensional (3-D), nonlinear finite element analysis using an elastic-plastic constitutive model were carried out.

2. EXPERIMENTAL AND ANALYSIS PROCEDURES

2.1. Experimental procedures

The solder balls used in this study had a composition of Sn-37Pb and Sn-3.5Ag (in mass percentage) and a diameter of 500 μm. As shown in Fig. 1, the substrate was a solder mask defined-type FR4 laminate with subsurface solder bond pads whose nominal size and shape were defined through a 460 μm-diameter circular opening. The pads comprised an electroless-Ni immersion-Au layer over an underlying Cu pad with thicknesses of 0.15 μm and 7.0 μm, respectively. The solder balls were bonded to the FR4 substrate in a reflow process employing rosin mildly activated flux in an infrared four zone reflow machine (RF-430-N2, Japan Pulse Laboratory Ltd. Co.) with a maximum temperature of 255 for Sn-3.5Ag and 220 for Sn-37Pb during 60 s. The microstructures were observed with scanning electron microscopy (SEM), and the compositions of the resulting IMCs were measured by an energy dispersive spectrometer (EDS). High-speed shear testing was conducted using a glo-

Table 1. Examined shear speed conditions in the high-speed shear test

Shear height (μm)	Shear speed (m/s)		
50	0.01	0.1	1

bal bond tester (DAGE-4000HS, Richardson Electronics Ltd.) under various testing speeds. Terminologies such as shear speed and shear height are defined in Fig. 1, and the shear test conditions are given in Table 1. The fracture mode of each test site was examined after shear testing to evaluate the failure mode.

2.2. Finite element analysis

The 3-D elastic-plastic finite element modeling simulation methodologies were used to analyze the effects of the shear speed on the failure behaviors of the solder joints. Figure 1 shows the finite element analysis model for the high-speed ball shear test. The components of the finite element analysis model included every detail of the real package, which contained a solder ball, electrolytic-plated Ni layer, Cu pad, FR4 substrate, and polyimide solder mask to determine the highest degree of accuracy. All the components were modeled by 20-node structural solid elements (SOLID186). The shear ram was considered a rigid body. A feature in ANSYS using the surface-to-surface target element (TARGET170) and the contact element (CONTA174) was employed to simulate the contact between the shear ram and the solder ball. For the

Table 2. Linear elastic material properties for the BGA assemblies

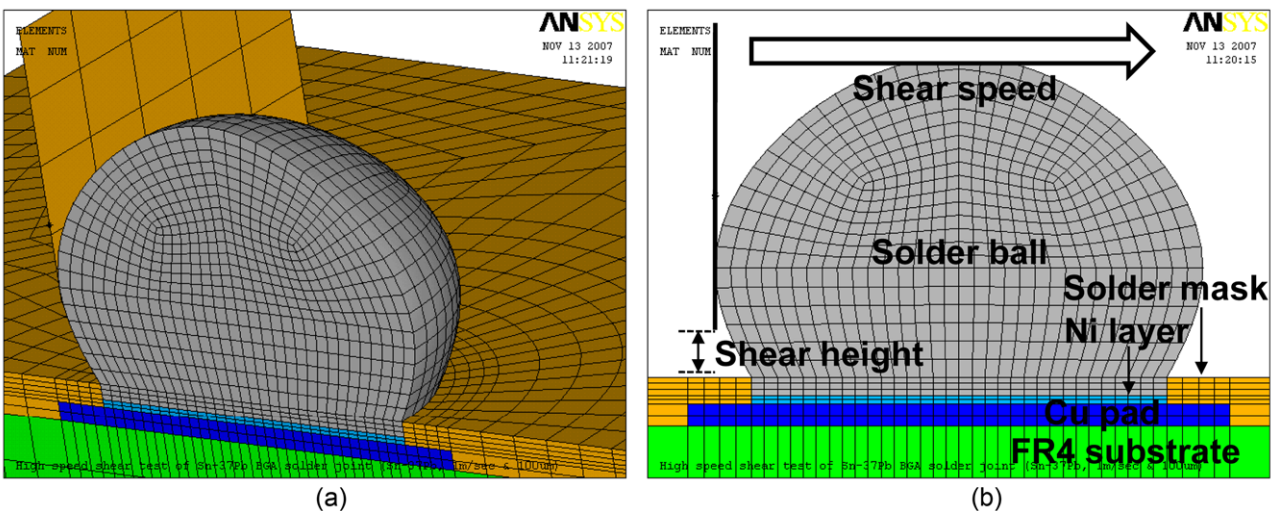| Materials	Young's Modulus (MPa)	Poisson's Ratio	Density (g/cm^3)
Sn-3.5Ag	49,800	0.40	7.5
Cu	117,000	0.34	8.9
Ni	213,000	0.31	8.9
Polyimide	4,200	0.16	1.6
FR4 Substrate	17,200	0.39	1.9

Fig. 1. Finite element model for the ball shear test (a) and enlarged view of the interfacial region (b).

plastic property of the solder, the multilinear isotropic hardening model using von Mises plasticity was employed. The properties of the materials other than the solder, which were treated like linear elastic materials, are listed in Table 2.

3. RESULTS AND DISCUSSION

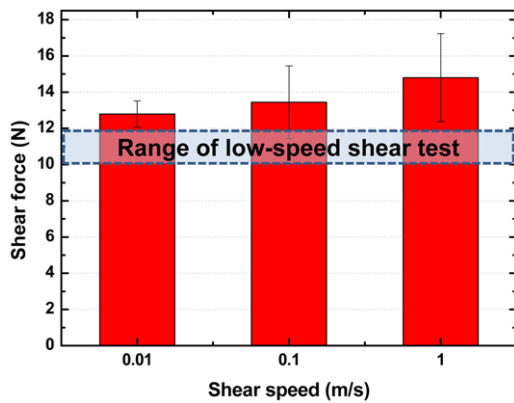Figure 2 shows the shear force variation of the Sn-3.5Ag solder joints under increasing shear speed in the high- and low-speed shear tests. The conditions for the low-speed shear test are a fixed shear height of 50 μm with a shear speed range of 10 μm/s to 700 μm/s. Twenty solder balls were sheared to failure for each test condition. As can be seen in Fig. 2, the shear force increased with increasing shear speed to a maximum at the highest shear speed. The shear forces measured by the high-speed shear test were much higher than those of the low-speed shear test, indicating that the increase in shear force with increasing shear speed was a direct consequence of the material properties, including both the time-independent plastic hardening and time-dependent strain-rate sensitivity. This could be supported only by the fact that the shear force is dominantly affected by the deformation of the mere solder. If the shear behavior is caused by a fracture at the interfacial region, this explanation should be reconsidered, so the investigation of the fracture surfaces of the solder joints sheared is essential. The rate-dependent plasticity and high speed loading has been discussed with various constitutive models, such as Nadai, Johnson-Cook, Zerilli-Armstrong, Bodner-Partom, and Cowper-Symonds
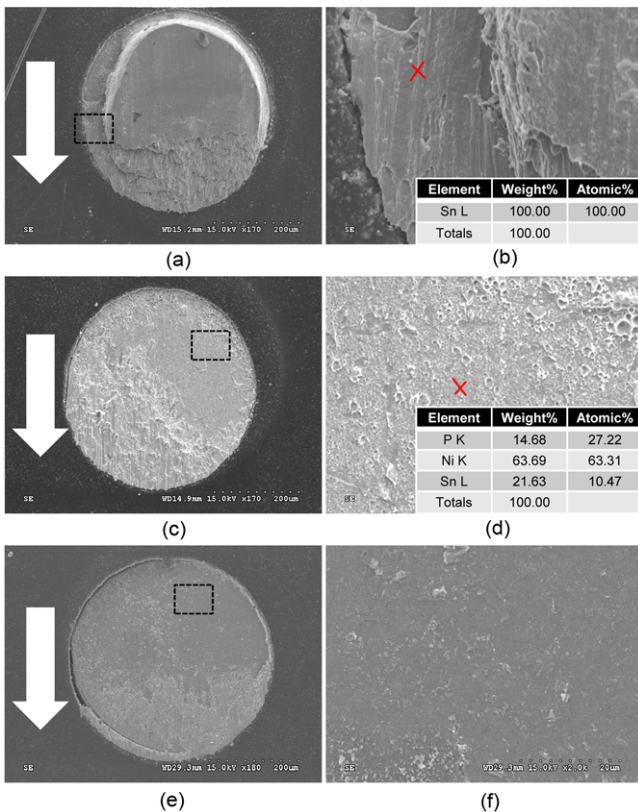

Fig. 2. Shear force variation of Sn-3.5Ag solder joints with shear speed ranging from 0.01 m/s to 1 m/s.

Fig. 3. Fracture surfaces of the Sn-3.5Ag BGA solder joints after high-speed shear testing under various shear speeds: (a) and (b) 0.01 m/s; (c) and (d) 0.1 m/s; (e) and (f) 1 m/s.
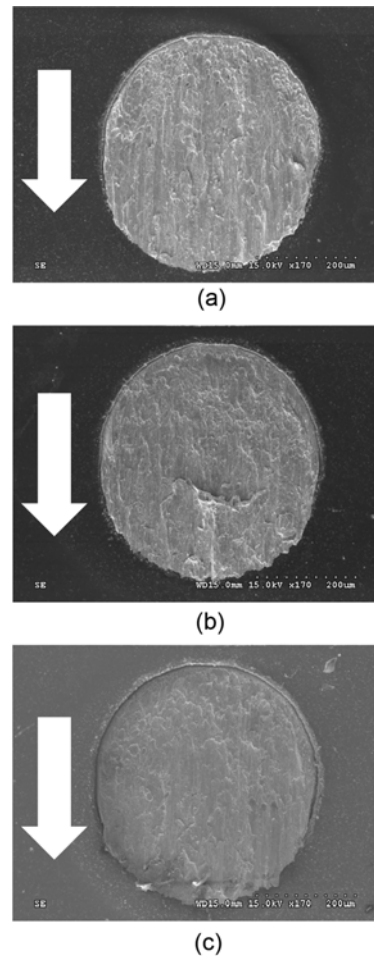

Fig. 4. Fracture surfaces of the Sn-37Pb BGA solder joints after high-speed shear testing under various shear speeds: (a) 0.01 m/s, (b) 0.1 m/s, and (c) 1 m/s.

[11-16]. Another point we should note in Fig. 2 is that the standard deviation values of 0.1 m/s and 1 m/s are much higher than that of 0.01 m/s, indicating that the shear speeds of 0.1 and 1 m/s might be some transition points of the fracture mode from ductile to brittle mode. Therefore, we investigated the fracture surfaces after the high-speed shear test.

Figure 3 shows the fracture surfaces of the Sn-3.5Ag solder ball joints after high-speed shear testing under various shear speeds. Ductile solder ball fractures occurred at 0.01 m/s, while brittle interfacial fractures of the IMC layers occurred partially or totally at 0.1 m/s and 1 m/s. From the EDS compositional analyses, the products in the brittle fractured regions were based on the electroless-plated Ni-P containing some Sn or Ni_3Sn_4 IMC. However, as shown in Fig. 4, only the ductile solder ball fracture was observed on the sheared Sn-37Pb solder joints, regardless of the shear speed applied. Figs. 5(a)-(c) and (d)-(f) show the failure mode distributions of the Sn-3.5Ag and Sn-37Pb solder joints, respectively, at various shear speeds. The transition from the ductile solder ball fractures at a lower shear speed to brittle IMC fractures at a higher shear speed is clearly seen in the Sn-3.5Ag, but not the Sn-37Pb, solder joints. This difference was explained by Figs. 6(a) and (b), which demonstrate the failure mechanisms of the Pb-bearing and Pb-free solder joints, respectively. As shown in Fig. 6(a), the deformation of the solder, which is mainly caused by the relatively soft nature of the Pb-bearing solder, releases the shear-induced stress within the solder joint by allowing some plastic deformation. Therefore, only a small amount of stresses could be transferred from the bulk solder to the interfacial region when the soft
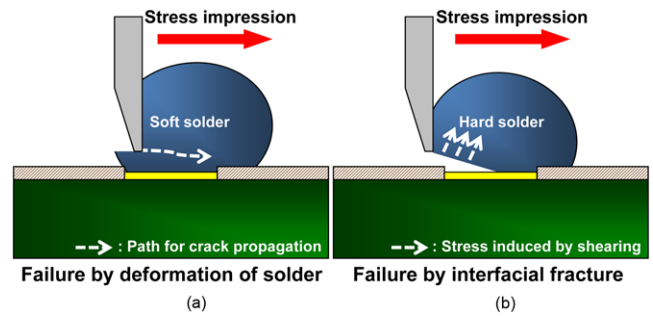

Fig. 6. Schematics of failure mechanisms under high-speed loading: (a) soft and (b) hard solders.

solder was used for bumping. On the other hand, as shown in Fig. 6(b), the solder was barely deformed in the plastic range when hard solder alloys such as Sn-based, Pb-free solders were used for bumping. Therefore, the shear-induced stress could easily be transferred from the solder to the interfacial areas, leading to the brittle fracture of the solder joints. This mechanism explained the different failure behaviors of the Sn-37Pb and Sn-3.5Ag solder joints under high-speed loading. As the Sn-3.5Ag solder joint did not exhibit the failure mode transition in the low-speed shear test with increasing shear speed, it could also be said that the high-speed shear test was more susceptible to brittle interfacial fractures by dynamic loading.

To analyze the fracture mode transition with increasing shear speed, finite element modeling was conducted. Figs. 7(a) and (b) show the distributions of the averaged incremental equivalent plastic strain in a cross-sectional view of
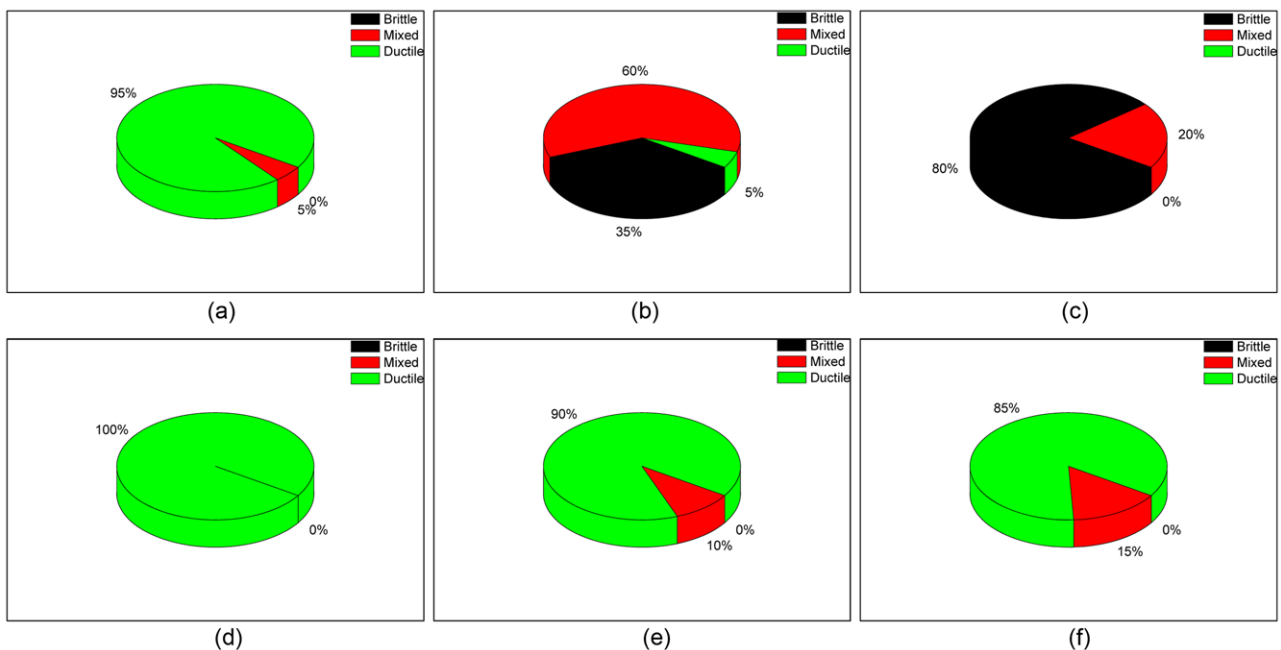

Fig. 5. Fracture mode distributions of Sn-3.5Ag (a-c) and Sn-37Pb (d-f) solder joints after high-speed shear testing under various shear speeds: (a) and (d) 0.01 m/s, (b) and (e) 0.1 m/s, (c) and (f) 1 m/s.
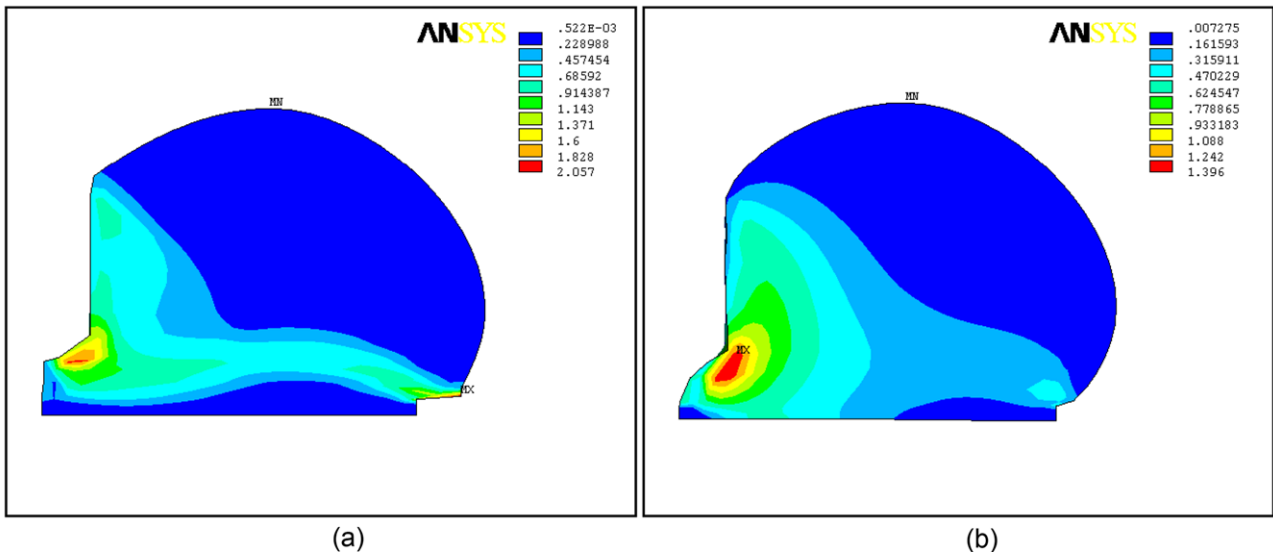
Fig. 7. Finite element modeling analysis results: contour plots of averaged equivalent plastic strain after shearing at a shear speed of (a) 0.01 m/s and (b) 1 m/s.
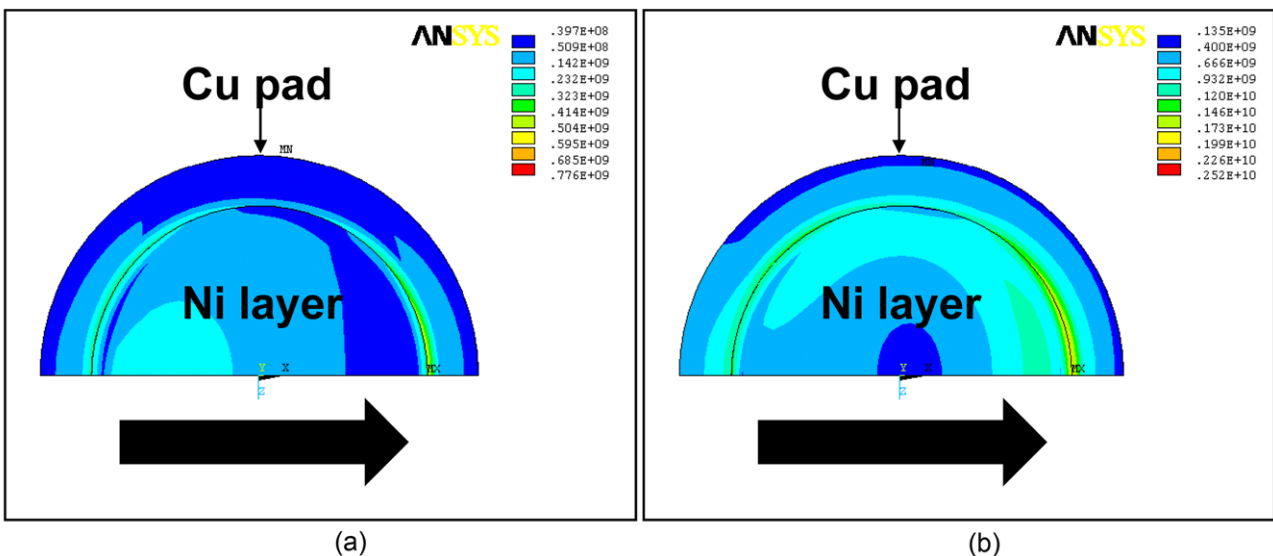

Fig. 8. Finite element modeling analysis results: contour plots of von-Mises stresses on Ni-plated Cu pad after shearing at a shear speed of (a) 0.01 m/s and (b) 1 m/s.

the solder joints, while Figs. 8(a) and (b) show the distributions of von-Mises stress in the top views of the Ni-plated Cu pads. With the equivalent plastic strain distribution, the solder ball joint sheared at a shear speed of 0.01 m/s was deformed more than that of 1 m/s (see the shape of the deformed solder balls). The overall values of the plastic strain also showed that the solder joint sheared at a lower loading speed was deformed more than that of a higher loading speed. The smaller strains at faster loading speeds were caused by the so-called work-hardening of the solder during deformation, whereby a higher strain-rate increases the dislocation density. The dislocation mobility is also low at high strain rates, which necessitates high stresses to develop plas-

tic deformation, and, thus, deformation twins further develop due to the high stresses [17,18]. In the case of a displacement controlled test, as we employed in this study, higher stresses should be induced in the solder joint at a high loading speed. However, because the bulk solder might be rather stiff at the high loading speed, it is difficult to release the stress that has built up during loading. Therefore, the stress is shifted to a nearby region such as an IMC layer or other weak layers.

In the von-Mises stress distributions shown in Figs. 8(a) and (b), the application of the shear loads to a multiphase structure results in the formation of a singularity phenomenon, i.e., a stress concentration, at the corner of the common boundary of two different materials (solder and Ni layer).
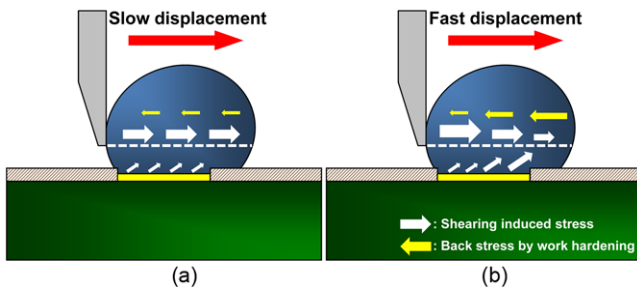
Fig. 9. Schematics of simplified stress field in the solder ball joint during high-speed shear test at (a) lower and (b) higher shear speeds.

This is due to the phase discontinuity that occurs at this boundary. In both of the shear speed cases, the maximum stressed region was located in the right corner of the Ni layer. However, much higher stresses, about one-order of magnitude larger, were distributed on the Cu pad and the plated Ni layer at higher shear speed. The higher stresses at the higher speed were caused by the stiffer solder ball during the shear test, which is consistent with the results of the plastic strain analyses. These results imply that the brittle interfacial fracture could be achieved more easily at higher shear speeds. Therefore, cases with higher shear speed could more easily screen the type of brittle interfacial fractures affected by dynamic loads. Figure 9 presents a schematic illustration of the stress field in the solder ball joint during the shear test. In comparison with the slow displacement of the shear probe, the shearing-induced stress should be decreased with the progress of shear probe displacement in the faster displacement case, and this is due to the increased back stress arising from the work hardening of the solder material. This could explain both the stress concentration at the interfacial region and the occurrence of brittle IMC fractures at higher shear speeds.

4. CONCLUSION

The effects of shear speed in the high-speed range on the failure behaviors and bonding forces of the Pb-bearing and Pb-free BGA solder joints were investigated. Both experimental results and computational simulations utilizing finite element modeling were used to analyze the failure mechanism. Far greater shear forces were measured by the high-speed shear test than by the low-speed shear test, and the shear force also increased with increasing shear speed in the high-speed shear test, mainly due to the high strain-rate sensitivity of the solder alloys. With the Sn-based, Pb-free solder (Sn-3.5Ag), brittle interfacial fractures were achieved more easily by the high-speed shear test, and the rate of brittle fracture occurrence increased with the increasing shear speed in the high-speed shear test. This was attributed to the relationship between the strain-rate and work-hardening effect, i.e., the higher stresses induced by the work-hardened solder ball in high-speed shearing were transferred to the interfacial

regions as a stress concentration. However, the transition of the failure mode was not observed in the Sn-37Pb solder joint due to its soft nature. The high stresses were released by allowing plastic deformation in the solder, and, thus, only a small amount of stresses were concentrated at the interface.

REFERENCES

1. A. R. Zbrzezny, P. Snugovsky, and D. D. Perovic, *Microelectron. Reliab.* **47**, 2205 (2007).
2. Y. S. Lai, P. F. Yang, and C. L. Yeh, *Microelectron. Reliab.* **46**, 645 (2006).
3. F. Song, S. W. Ricky Lee, K. Newman, B. Sykes, and S. Clark, *Proc. of the 2007 Electronic Components and Technology Conference*, p. 364, IEEE, Reno, USA (2007).
4. E. Kaulfersch, S. Rzepka, V. Ganeshan, A. Muller, and B. Michel, *Proc. of the International Conference on Thermal, Mechanical and Multi-Physics Simulation Experiments in Microelectronics and Micro-Systems*, p. 1, IEEE, London, UK (2007).
5. B. Zhao, B. An, F. S. Wu, and Y. P. Wu, *Proc. of the 7th International Conference on Electronics Packaging Technology*, p. 1, IEEE, Shanghai, China (2006).
6. C. L. Yeh, Y. S. Lai, H. C. Chang, and T. H. Chen, *Microelectron. Reliab.* **47**, 1127 (2007).
7. JESD22-B117A, JEDEC Solid State Technology Association (2006).
8. J. W. Kim and S. B. Jung, *Int. J. Solids Struct.* **43**, 1928 (2006).
9. J. W. Kim and S. B. Jung, *Mater. Sci. Eng. A* **371**, 267 (2004).
10. J. W. Kim, D. G. Kim, and S. B. Jung, *Met. Mater. Int.* **11**, 121 (2005).
11. G. E. Dieter, *Mechanical Metallurgy*, p. 139, McGraw-Hill, New York (1988).
12. A. Nadai, *Theory of Flow and Fracture of Solids*, p. 535, McGraw-Hill, New York (1950).
13. G. R. Johnson and W. H. Cook, *Proc. of 7th International Symposium on Ballistics*, p. 541, Technomic. Pub. Co., Hague, Netherlands (1983).
14. F. J. Zerilli and R. W. Armstrong, *J. Appl. Phys.* **61**, 1816 (1987).
15. S. R. Bodner and Y. J. Partom, *J. Appl. Mech.* **42**, 385 (1975).
16. P. S. Symmonds, *Behaviour of Materials under Dynamic Loading*, p. 106, ASME, New York, USA (1965).
17. J. M. Koo and S. B. Jung, *Microelectron. Reliab.* **47**, 2169 (2007).
18. D. R. Chichili, K. T. Ramesh, and K. J. Hemker, *Acta mater.* **46**, 1025 (1998).